ELSEVIER

Pattern Recognition Letters 22 (2001) 35–46

Pattern Recognition Letters

www.elsevier.nl/locate/patrec

# Improved MR image reconstruction from sparsely sampled scans based on neural networks

M. Reczko [a], D.A. Karras [b,*], B.G. Mertzios [a], D. Graveron-Demilly [c], D. van Ormondt [d]

[a] *DEMOCRITUS University of Thrace, Xanthi, Greece*
[b] *Department of Business Administration, University of Piraeus, Ano Iliupolis, Rodu 2, 16342 Athens, Greece*
[c] *Laboratoire de RMN, CNRS, UPRESA 5012, Universite LYON I-CPE, France*
[d] *Applied Physics Department, Delft University of Technology, P.O Box 5046, 2600 GA Delft, The Netherlands*

**Abstract**

This paper concerns a novel application of machine learning to magnetic resonance imaging (MRI) by considering neural network models for the problem of image reconstruction from sparsely sampled *k*-space. Effective solutions to this problem are indispensable especially when dealing with MRI of dynamic phenomena since then, rapid sampling in *k*-space is required. The goal in such a case is to reduce the measurement time by omitting as many scanning trajectories as possible. This approach, however, entails underdetermined equations and leads to poor image reconstruction. It is proposed here that significant improvements could be achieved concerning image reconstruction if a procedure, based on machine learning, for estimating the missing samples of complex *k*-space were introduced. To this end, the viability of involving supervised and unsupervised neural network algorithms for such a problem is considered and it is found that their image reconstruction results are very favorably compared to the ones obtained by the trivial zero-filled *k*-space approach or traditional more sophisticated interpolation approaches. © 2001 Published by Elsevier Science B.V.

*Keywords:* Magnetic resonance imaging; Neural network; Machine learning

## 1. Introduction

The MR image is actually a map of the very weak magnetization, originated from some of the atomic nuclei in the body tissue, in the presence of an external magnetic field. Since this magnetization is proportional to the density of those nuclei, the MR image shows the distribution of the selected atoms. Because of the large hydrogen concentration, soft tissue is easily seen in proton MR images, that show even the small differences due to their different chemical composition. A data acquisition process is needed to form the MR images. Such data acquisition occurs in the spatial frequency (*k*-space) domain where sampling theory determines resolution and field of view. *k*-space is an imaginary space (comprising of complex values) whose coordinates are in terms of phase and frequency for conventional imaging and in terms of phase in 2 or 3 dimensions for 2-D and

* Corresponding author. Tel.: +30-944-226-018; fax: +30-199-45231.
*E-mail addresses:* dakarras@usa.net, dakarras@hotmail.com, dakarras@hol.gr (D.A. Karras).

0167-8655/00/$ - see front matter © 2001 Published by Elsevier Science B.V.
PII: S0167-8655(00)00097-0

3-D chemical shift imaging. The $k$-space matrix is to obtain the familiar spatial dimensions. Strategies for reducing image artifacts are often best developed in this domain. After obtaining such a $k$-space matrix, image reconstruction involves fast multi-dimensional inverse Fourier transforms, often preceded by data interpolation and re-sampling.

Sampling the $k$-space matrix occurs along suitable trajectories (Basic Principles of MR Imaging, 1995). Ideally, these trajectories are chosen to completely cover the $k$-space according to the Nyquist sampling criterion. The measurement time of a single trajectory can be made short. However, prior to initiating a trajectory, return to thermal equilibrium of the nuclear spins needs to be awaited. The latter is governed by an often slow natural relaxation process that is beyond control of the scanner and impedes fast scanning. Therefore, the only way to reduce scan time in magnetic resonance imaging (MRI) is to reduce the overall waiting time by using fewer trajectories, which in turn should individually cover more of $k$-space through added curvatures. This fast scanning approach in MRI is indispensable when dynamic phenomena are considered, as for instance, in functional MRI. Although, however, such trajectory omissions achieve the primary goal, i.e., more rapid measurements, they entail undersampling and violations of the Nyquist criterion thus, leading to concomitant problems for image reconstruction.

The above mentioned rapid scanning in MRI problem is highly related with two other ones. First is the selection of the optimal scanning scheme in $k$-space, i.e., the problem of finding the shape of sampling trajectories that more fully cover the $k$-space using fewer number of trajectories. Second one is associated with image estimation from fewer samples in $k$-space, i.e., the problem of omitting as many trajectories as possible without attaining worse results concerning image reconstruction.

Regarding the former issue, mainly three alternative shapes of sampling trajectories have been considered in the literature and are used in actual scanners, namely, Cartesian, radial and spiral (Stijnman et al., 1997). The last two of them are shown in Fig. 1, presenting different advantages and disadvantages.

Both Cartesian and radial trajectories are straight lines. However, the former start at edge of $k$-space where the signal is weakest, whereas the latter start at the centre of $k$-space where the signal is strongest. An obvious advantage of Cartesian scanning is that all sample positions coincide with a uniform rectangular grid, allowing very fast image reconstruction simply using the inverse 2-D FFT. Advantages of radial scanning are: less sensitivity to motion of the patient and the ability to deal with possible very fast decays of signals. A disadvantage of radial scanning is that the data are not amenable to direct application of the inverse 2-D FFT, which significantly slows

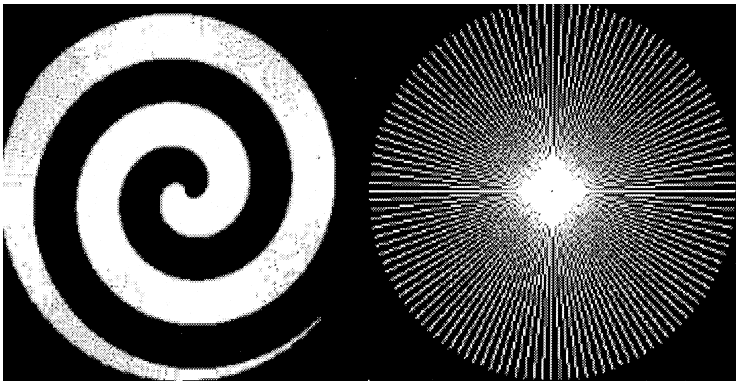

Fig. 1. Spiral (left) and radial (right) scanning trajectories in $k$-space (white area). For the spiral sampling, out of 60 trajectories covering the complete $k$-space, the first 30 trajectories are omitted, while for the radial only 128 trajectories have been sampled.

down the reconstruction process. In this case, the image can be obtained by using the Projection Reconstruction approach (Stijnman et al., 1997), the linogram method (Stijnman et al., 1997) or the SRS–FT (Stijnman et al., 1997) approach. Finally, spiral trajectories, being strongly curved, cover much more $k$-space than Cartesian and radial trajectories do. As a result, fewer spirals are needed to satisfy the Nyquist sampling criterion everywhere.

Concerning the second issue, the main result of the scan trajectories omissions is that we have fewer samples in $k$-space than needed for estimating all pixel intensities in image space. Therefore, there is an infinity of MRI images that satisfy the sparse $k$-space data and thus, the reconstruction problem becomes ill-posed. Additionally, omissions usually cause violation of the Nyquist sampling condition. Despite the fact that solutions to this second problem are urgently needed, in functional MRI, for instance, very few research efforts exist in the literature. Several approaches, however, could be applied to cope with the image reconstruction problem from sparse $k$-space data. The most obvious and simplest such method is the so called "zero-filling the $k$-space", i.e., all missing points in $k$-space acquire complex values equal to zero. Subsequently, image reconstruction is achieved as usual, by applying the inverse Fourier transform to the corresponding $k$-space matrix. Instead of zero-filling the $k$-space, it might be more advantageous to interpolate it by using linear and nonlinear interpolation procedures. This is precisely the approach investigated in this paper. More specifically, novel machine learning based interpolation techniques are proposed and evaluated in the following sections.

The organization of this paper is as follows. Section 2 discusses the need for alternative strategies in the problem of MRI reconstruction from sparse $k$-space matrices. In Sections 3 and 4 the proposed methodology is illustrated. In Section 5 the experimental study exhibiting the comparisons of the various interpolation techniques herein involved in MRI reconstruction, is presented and the results obtained are discussed. Finally, Section 6 concludes the paper.

## 2. Alternative strategies for estimating the missing samples in $k$-space

The above discussed problems of ill-posed MRI reconstruction from sparse $k$-space might be amended by using the so-called Bayesian reconstruction approach recently proposed by two of the authors (Stijnman et al., 1997), through regularizing the problem by invoking general prior knowledge in the context of Bayesian formalism. The algorithm amounts to minimizing the following objective function (Stijnman et al., 1997),

$$\begin{aligned} &| \boldsymbol{S} - T\boldsymbol{I} |^2 / (2\sigma^2) \\ &\quad + (3/2) \sum_{x,y} \log \left\{ \alpha^2 + ({}^{x}\Delta_{xy})^2 + ({}^{y}\Delta_{xy})^2 \right\}, \end{aligned} \tag{1}$$

with regards to $\boldsymbol{I}$, which is the unknown image to be reconstructed that fits to the sparse $k$-space data given in $\boldsymbol{S}$. First term comes from the likelihood term and the second one from the prior knowledge term of the well-known Bayesian formulation (Stijnman et al., 1997). In the above formula, $T((k_x, k_y), (x, y)) = e^{-2\pi i(xk_x + yk_y)}$ represents the transformation from image to $k$-space data (through 2-D FFT). Second term symbols arise from the imposed 2-D Lorentzian prior knowledge. ${}^{x}\Delta_{xy}$ and ${}^{y}\Delta_{xy}$ are the pixel intensity differences in the $x$- and $y$-directions, respectively, and $\alpha$ is a Lorentz distribution-width parameter. If we assume that $P(I)$ is the prior, which imposes prior knowledge conditions about the MRI image on the reconstruction algorithm, then, the second term of (1) comes as follows.

The starting point is that $P(I)$ could be obviously expanded into $P(I) = P(I_{0,0})P(I_{1,0}\,|\,I_{0,0})$ $P(I_{2,0}\,|\,I_{0,0}, I_{1,0}) \ldots$. If, now, it is assumed that the intensity $I_{x,y}$ depends only on its left neighbor $(I_{x-1,y})$, then the previous $P(I)$ expansion takes on the form $P(I) = \prod_{(x,y)} P(I_{x,y}\,|\,I_{x-1,y})$, provided that the boundaries are ignored. Next, we assume that $P(I_{x,y}\,|\,I_{x-1,y})$ is a function only of the difference between the corresponding pixels. This difference is written down as ${}^{x}\Delta_{xy} = I_{x,y} - I_{x-1,y}$. It has been shown that the probability density function of ${}^{x}\Delta_{xy}$ is Lorentzian shaped (see Fuderer, 1989; Herbert and Leahy, 1989; Lettington and Quong, 1995). These assumptions and calculations lead directly

to compute the prior knowledge in the Bayesian reconstruction approach as in (Eq. 1).

Although the Bayesian reconstruction approach tackles the problem of handling missing samples in $k$-space, it exhibits, however, some disadvantages. First, the validity of the assumption that the Gaussian probability distributions involved in this method are adequate for formulating the probability distributions occurred in any MRI image is an issue under question. Second, the fact that Bayesian formulation of the problem treats it as being an optimization problem could lead to inferior reconstruction results. Indeed, as it was discussed above, after the Bayesian formulation of the reconstruction task in MRI, the conjugate gradient method is applied to the corresponding objective function in order to find its optima. Conjugate gradients, which is a local optimization technique, has been invoked here as the optimization procedure of preference since a huge number of variables is actually involved (all $N \times N$ image pixels). It is well-known, however, that local optimization procedures can usually get stack to some local optima of the objective function, been unable to find the desired global optimum. Their performance depends on the initial values of the design variables. On the other hand, even if global optimization techniques were invoked there would be no guarantee, in the general case, that the global optimum could be reached. Therefore, the optimization formulation of the MRI reconstruction from missing samples cannot ensure the quality of the resulted image by its own, but it depends, instead, on the quality of the initial conditions for the design variables. Third, the fact, again, that the Bayesian reconstruction approach leads to a formulation in terms of an extremely huge optimization problem has as another consequence, the need for immense computing power and storage requirements. The above disadvantages worsen things when 3-D Bayesian MRI reconstruction is considered, especially in the case of functional MRI. In this case a lot of slices should be acquired in order to have a 3-D reconstruction and the problem of reducing scan time by omitting scanning trajectories becomes of primary importance.

The previous discussion makes obvious that another more effective methodology for handling the reconstruction problem in the sparse sampled $k$-space is needed and this is exactly the motivation for the research presented here. The methodology herein suggested is based on the attempt to fill in the missing complex values in $k$-space from their neighboring complex values. This approach transforms the original problem into an interpolation one in the complex domain. While linear interpolators have already been used in the literature (Smith et al., 1986; Barone and Sebastiani, 1992; Dologlou et al., 1996) and nonlinear estimations are well established in MRI (Li and Hornak, 1994; Servoss and Hornak, 2000), the novelty of this paper lies on the fact that it deals with nonlinear interpolation in $k$-space. The obvious advantages of the interpolation approach compared to the Bayesian formalism are the capability for faster reconstruction since it avoids optimization procedures during reconstruction, the need for less computing power and fewer storage requirements as well as the avoidance of any model assumption about the probability distributions. This last point is ensured because of the application of artificial neural network (ANN) models in the complex domain interpolation task herein involved. The reconstruction results achieved by both supervised architectures of the MLP type and unsupervised ones of the Kohonen type are very promising and very favorably compared to the reconstruction results obtained by traditional interpolation techniques as well as by the simplest "interpolation" procedure, that is by zero-filling the missing samples in $k$-space. Finally, an initial comparison with the Bayesian reconstruction approach indicates that ANN is a good candidate for offering a viable solution to the problem of $k$-space interpolation.

## 3. Training supervised and unsupervised neural networks for estimating the missing samples in $k$-space

The training phase of the neural models involved in the proposed interpolation procedure for predicting missing complex values in the $k$-space from their surrounding, is outlined in the following steps.

We compile a set of $R$ representative $N \times N$ MRI images with $k$-space matrices completely known, which comprise the training set of the neural interpolators. Subsequently, we scan these matrices by following either radial or spiral sampling schemes as shown in Fig. 1 and discussed in the introduction. Afterwards, for each image of the training set, its corresponding sparse $k$-space is constructed from the original $k$-space matrix by excluding all points not belonging to the sampling trajectories. We keep, however, the original $k$-space intact in order to extract from it the desired patterns defined next. All the missing $k$-space samples take on complex values of zero. Thus, the corresponding sparse $k$-space is zero-filled.

The original $k$-space matrix as well as its corresponding sparse $k$-space matrix associated with one $N \times N$ MRI image, belonging in the previously defined training set, is raster scanned by a $(2M+1) \times (2M+1)$ sliding window containing the associated complex $k$-space values. The estimation of the complex number in the center of this window from the rest of the complex numbers comprising the sliding window is the goal of the proposed interpolation procedure (either in the original $k$-space or in the sparse one). Each position of the previously defined sliding window in $k$-space (original or sparse) is, therefore, associated with a desired output pattern comprised of the complex number in the *original k-space* corresponding to the window position, and an input pattern comprised of the complex numbers in $k$-space corresponding to the rest $(2M+1)\times(2M+1)-1$ window points. This scheme is used in the MLP case, while in the Kohonen's self-organizing feature map (SOFM) case there is only an input pattern with $(2M+1) \times (2M+1)$ complex number components. The following table illustrates how the input pattern - desired output pattern pair is defined for a specific sliding window ($5 \times 5$), raster scanning either the sparse or the original $k$-space of an MRI image. In this table, I stands for a $k$-space point (complex value) belonging in the scanning trajectories, while $\times$ stands for a $k$-space point not belonging in them (Don't care state. It equals zero or any other complex value. The reason for including such states in the training patterns is to enhance the generalization capability of neural interpolators, since this is actually the form of the real world test input patterns). Finally, $D$ stands for the desired output pattern (a complex value) of the MLP neural model, provided by the original $k$-space matrix. For instance, the MLP input pattern associated with this table is ($I$, $I$, $I$, $X$, $X$, $X$, $X$, $I$, $I$, $I$, $I$, $I$, $I$, $X$, $I$, $I$, $I$, $I$, $X$, $I$, $X$, $I$, $I$, $I$) starting from the first row and moving from left to right to construct it. The associated desired output is simply equal to $D$.

| | | | | |
|---|---|---|---|---|
| $I$ | $I$ | $I$ | $X$ | $X$ |
| $X$ | $X$ | $I$ | $I$ | $I$ |
| $I$ | $I$ | $D$ | $I$ | $X$ |
| $I$ | $I$ | $I$ | $I$ | $X$ |
| $I$ | $X$ | $I$ | $I$ | $I$ |

Each such pattern is then, normalized according to the following procedure. First, the absolute values of the complex numbers in the input pattern are calculated and then, their average absolute value $|z_{\text{aver}}|$ is used to normalize all the complex numbers belonging both in the input and the desired output patterns. That is, if $z_1$ is such a number then this normalization procedure transforms it into the $z_1/|z_{\text{aver}}|$ . This pair of normalized input and desired output patterns of complex $k$-space values can be next used in the training procedure of the ANN interpolation architecture. On the other hand, in the case of test patterns we apply the same procedure. That is, the average absolute value $|z_{\text{aver}}|$ for the complex numbers of the test input pattern is first calculated and used to normalize them. Afterwards, these normalized complex values $z_i/|z_{\text{aver}}|$ feed the ANN interpolation technique to predict the sliding window central normalized complex number $z^{\text{norm}}_{\text{centre}}$. The corresponding unnormalized complex number is simply $z^{\text{norm}}_{\text{centre}} * |z_{\text{aver}}|$.

The next step is the production of training patterns for the ANN interpolators. To this end, we involve the set of the above selected $R$ representative MRI images as training pictures and their corresponding $k$-space data. Then, by randomly selecting sliding windows from the associated $k$-spaces (the original and their associated sparse ones) and producing the corresponding

input and desired output training pairs of patterns, as previously defined, we construct the set of training patterns. The assumption that underlies such an approach of training ANN interpolators is that there are regularities in every sliding window associated $k$-space data, the same for any MRI image, which can be captured by the ANNs. Unlike Bayesian reconstruction, however, this can be achieved without any prior assumption for the model of their probability distributions.

In the sequel, the ANN interpolators are trained using the previously defined learning sets. In the case of the MLP based complex interpolator both input and desired output patterns are involved. Each complex number, component of either an input or an output pattern, is associated with two adjacent neurons of the MLP input or output layer respectively, having its real part assigned to the left neuron of the pair and its imaginary part to the right one. The same assignments for the complex numbers belonging to the input training patterns are met in the case of the Kohonen's SOFM. However, since this is an unsupervised architecture there is no desired output response employed in its training phase. Instead, the SOFM is comprised of an $L \times P$ array of output neurons that map the probability distribution of the $(2M+1) \times (2M+1)$ complex numbers of any input pattern, preserving the topological conditions of the input pattern space. That is, the training phase of the SOFM attempts to assign every input pattern to a neuron of the map so that the quantization error becomes as small as possible.

## 4. The neural networks based MRI image reconstruction

After completion of the above defined training procedure both supervised and unsupervised ANN interpolators can be evaluated by applying them to the sparse $k$-space data corresponding to a completely unknown set of MRI images. This application involves the following procedure.

(1) The $(2M+1) \times (2M+1)$ sliding window raster scans the sparse $k$-space data starting from the center. Its central point position moves along the perimeter of rectangles covering completely the $k$-space, having as center of gravity the center of the $k$-space array and having distance from their two adjacent ones of 1 pixel. It can move clockwise or counterclockwise or in both directions. For every position of the sliding window, the corresponding input pattern of $(2M+1) \times (2M+1) - 1$ or $(2M+1) \times (2M+1)$ complex numbers is derived following the above described normalization procedure.

(2) Subsequently, this normalized pattern feeds the ANN interpolator, either MLP or SOFM. In the case of MLP, the wanted complex number corresponding to the sliding window center, is found as $z_{\text{centre}} = z_{\text{MLP}}^{\text{out}} * |z_{\text{aver}}|$, where $z_{\text{MLP}}^{\text{out}}$ is the MLP output and $|z_{\text{aver}}|$ the average absolute value of the complex numbers comprising the unnormalized input pattern. In the case of SOFM, for the winning neuron corresponding to the test input pattern, its associated weight vector $\boldsymbol{W}^{\text{win}}$ might be considered as good representative of the cluster of input patterns that correspond to it. Then, the wanted complex number $z_{\text{centre}}$ is equal to $z_{\text{centre}} = (W_{x0}^{\text{win}}, W_{y0}^{\text{win}})$, where $W_{x0}^{\text{win}}, W_{y0}^{\text{win}}$ are the weights corresponding to the central values of the input pattern and the associated central point $(x0,\ y0)$ of the sliding window. Following this procedure, the unknown complex number that corresponds to the current sliding window position can be interpolated from its neighboring points values.

(3) For each rectangle covering the $k$-space, the previously defined filling in process takes place so that it completely covers its perimeter, only once, in both clockwise and counterclockwise directions. The final missing complex values are estimated as the average of their clockwise and counter-clockwise obtained counterparts.

At this point it should be mentioned that there is possibility for the ANN interpolators to estimate wrongly the missing complex values of the sliding window central positions. Then, of course, these errors propagate to all the following such estimations. However, fortunately, the problem is not too hard as it seems to be at first glance. This is because the missing points in the area near the center of $k$-space, where the signal is strongest, are few, irrespectively to the sampling scheme

involved. On the other hand, in the areas far from the center of $k$-space, where the signal is weak and is not as rich in information content as near the center, the population of missing points increases quickly with distance. Therefore, in the rich in information content $k$-space areas, ANN interpolators are less prone to significant error propagation as in the rest of $k$-space, where the propagation of error could be large. In addition, error propagation effects are reduced in our approach since we involve both clockwise and counter-clockwise estimation processes and we calculate the missing $k$-space samples as the averages of both these estimation results. It could be speculated and, probably analytically proved, that this averaging estimation procedure reduces the overall propagation error. The experimental section shows that this procedure leads to very good reconstruction results.

## 5. Experimental study

An extensive experimental study has been conducted in order to evaluate the above described ANN interpolation methodology. All the interpolation methods involved have been applied to a large MRI image database which has been downloaded from the Internet, namely, the Whole Brain Atlas (http://www.med.harvard.edu/AANLIB/home.html) (copyright © 1995–1999 Keith A. Johnson and J. Alex Becker). There exists the permission that portions of that database might be individually downloaded, copied, and cited for the personal and educational purposes of individuals and organizations in their work, provided that proper attribution and context are given. We have used three images, shown in Fig. 2, for training the ANN interpolators, and four images, shown in Figs. 3–8, for testing them. All these images have 256 by 256 dimensions. The $k$-space data for these images have been produced by applying the 2D FFT to them. Radial and spiral trajectories have been used to scan the resulted $256 \times 256$ complex array of $k$-space data. In the case of radial scanning $4 \times 256 = 1024$ radial trajectories are needed to completely cover $k$-space. On the other hand, in the case of spiral scanning 60 spirals are enough for attaining a good image reconstruction. In order to apply the interpolation techniques involved in this study, the $k$-space has been sparsely sampled using 128 only radial trajectories in the former case and 30 only spiral trajectories in the latter. Regarding the sliding window raster scanning the $k$-space, the best results were obtained using a $5 \times 5$ window for the MLP case and a $3 \times 3$ in the SOFM case.

Concerning ANN architectures, the best results for the MLP based interpolator have been achieved using an architecture of 48 input neurons,

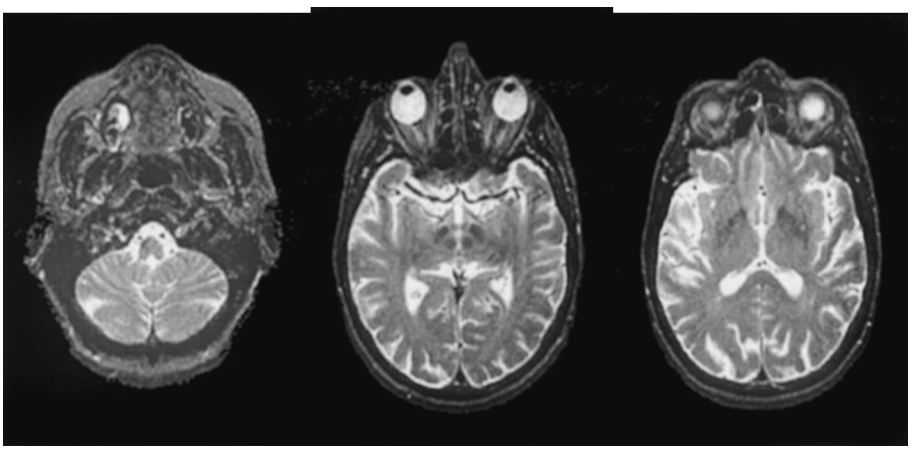

Fig. 2. From left to right: Training images, normal brain, 3 slices out of the complete database (http://www.med.harvard.edu/AANLIB/cases/caseM/mr1/008.html, 024.html, 028.html).

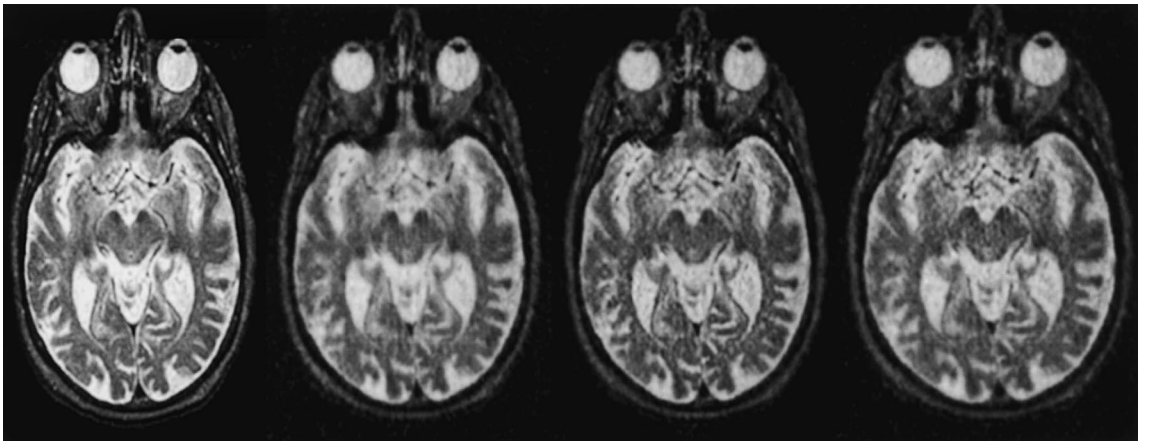

Fig. 3. From left to right: A test image illustrating a brain slice with Alzheimer's disease (http://www.med.harvard.edu/AANLIB/cases/case3/mr1-tc1/020.html), the sparsely sampled $k$-space ($nr = 128$) zero-filled image reconstruction, the BP-interpolated image and the Kohonen network estimated image.

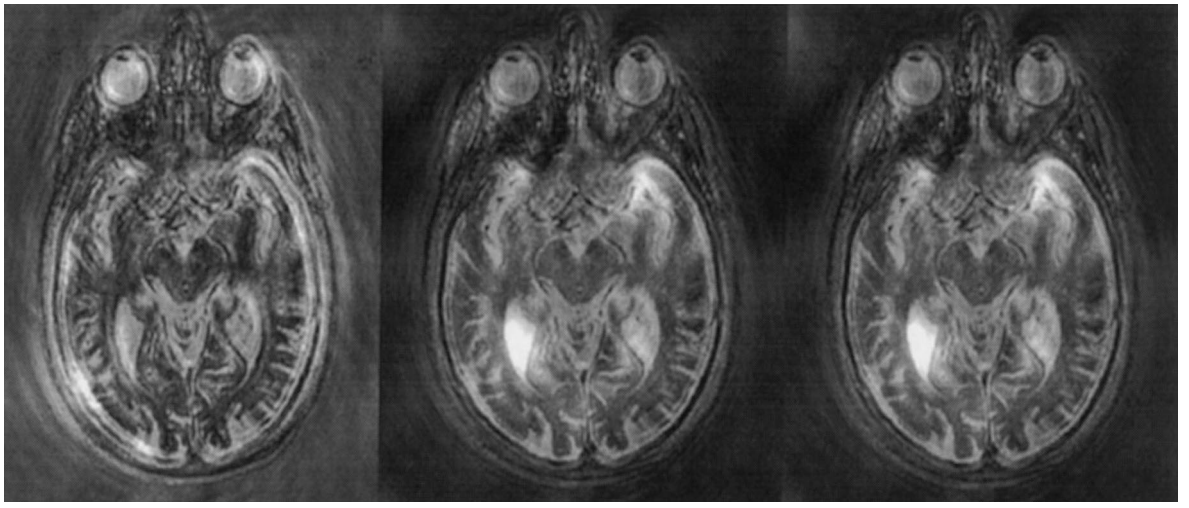

Fig. 4. From left to right: The test image of Fig. 3, the sparsely sampled on 30 spiral trajectories–zero-filled image reconstruction, the BP-interpolated image and the Kohonen network estimated image.

10 hidden ones and 2 output neurons. On the other hand, concerning the SOFM interpolator the best results have been obtained using an architecture of 18 input neurons and $25 \times 10$ output neurons in the map. These ANN interpolators have been trained using 3600 training patterns. Apart from the neural interpolators there was experimentation using two traditional interpolation techniques, namely, the linear and the cubic one. Moreover, the simplest "interpolation" approach, namely filling in the missing samples in $k$-space with zeroes and then, reconstructing the image, has been invoked. Finally, we have added an initial experimentation with the Bayesian reconstruction approach. All these methods (2 neural, 2 traditional, Bayesian and the zero-filling based reconstruction) have been implemented in the MATLAB programming language and all simulations have

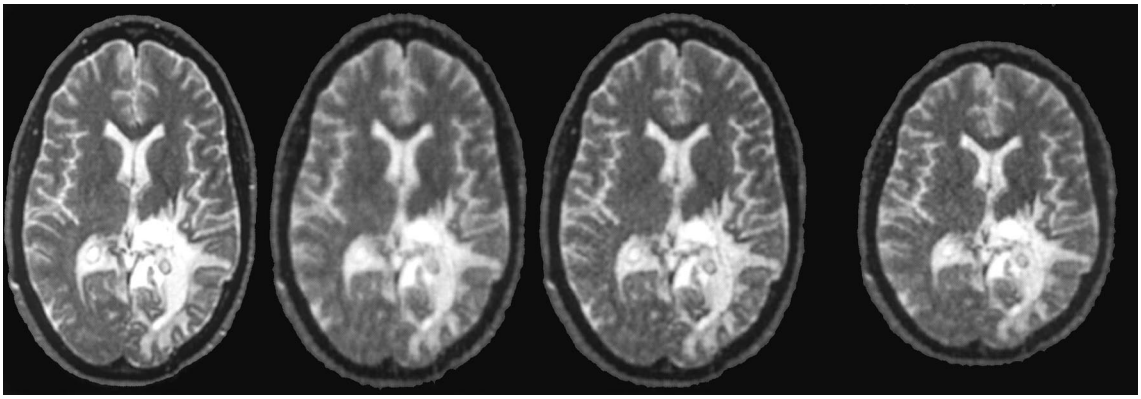

Fig. 5. From left to right: A test image showing a brain with Glioma (brain-tumor)-TlTc-SPECT (http://www.med.harvard.edu/AANLIB/cases/case1/mr1-t14/029.html), the zero-filled image reconstruction, the BP-interpolated image and the Kohonen network estimated image.

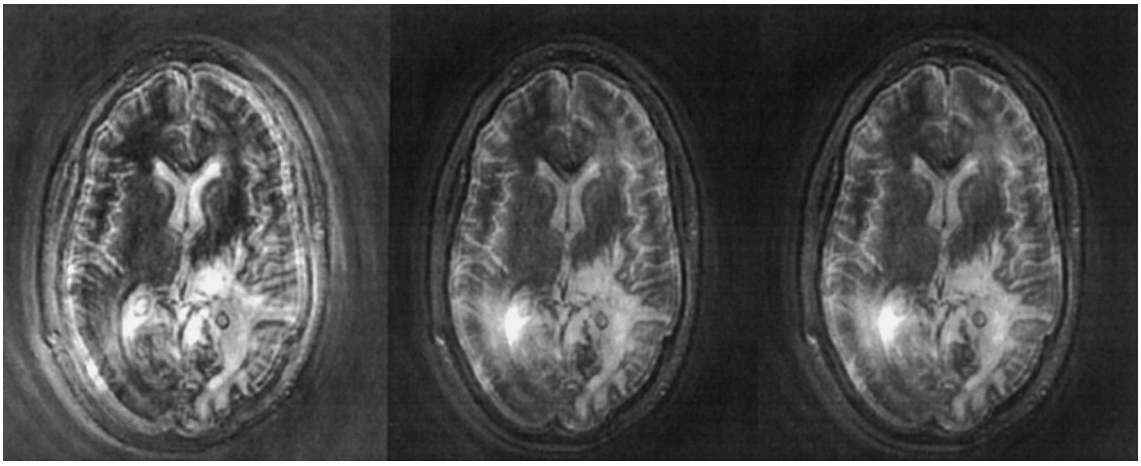

Fig. 6. From left to right: The test image of Fig. 5 sparsely sampled on 30 spiral trajectories, the zero-filled image reconstruction, the BP-interpolated image and the Kohonen network estimated image.

been carried out using the MATLAB programming platform.

Concerning the measures involved to quantitatively compare the performance of the various interpolation techniques, we have employed the usually used sum of squared errors (SSE) between the original MRI image pixel intensities and the corresponding pixel intensities of the reconstructed image. Additionally, another quantitative measure has been used, which expresses performance differences in terms of the RMS error in dB. This is outlined in the following MATLAB code and has been proposed in Dologlou et al., 1996

$$\text{lambda} = (\text{image\_recon}(:)' * \text{image\_orig}(:))/(\text{image\_recon}(:)' * \text{image\_recon}(:));$$

$$\text{residu} = \text{image\_orig} - \text{lambda} * \text{image\_recon};$$

$$\text{dB} = 10 * \log10((\text{image\_orig}(:)' * \text{image\_orig}(:))/(\text{residu}(:)' * \text{residu}(:)));$$

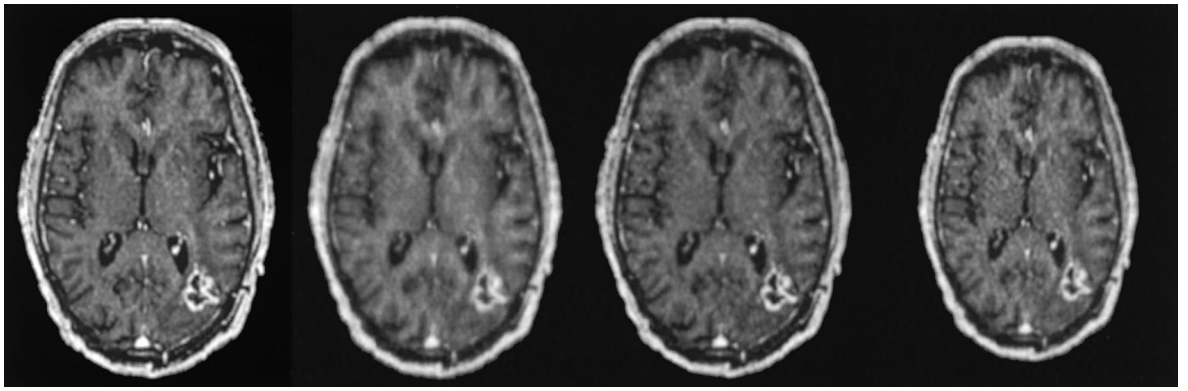

Fig. 7. From left to right: A test image – Glioma (brain-tumor)-FDG-PET (http://www.med.harvard.edu/AANLIB cases/caseSLU/mr1-dg1/060.html), the zero-filled image reconstruction, the BP-interpolated image and the Kohonen network estimated image.

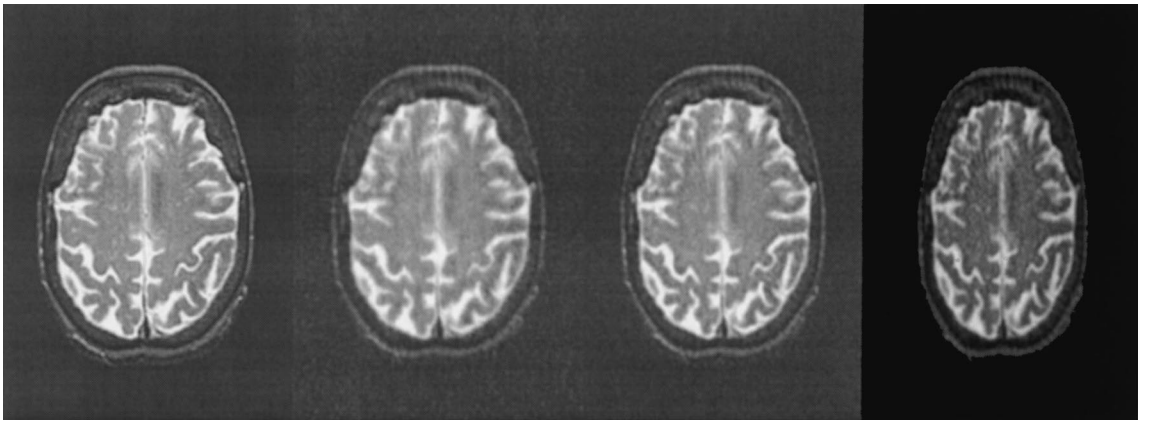

Fig. 8. From left to right: A Test image showing a normal brain slice 38-(http://www.med.harvard.edu/AANLIB/cases/caseM/mr1/0.38.html), the zero-filled image reconstruction, the BP-interpolated image and the Kohonen network estimated image.

Table 1
The quantitative results with regards to reconstruction performance of the various methodologies involved

| Test picture | Sampled trajectories | Bayesian | | Zero-filled | | Kohonen model | | MLP network | |
|---|---|---|---|---|---|---|---|---|---|
| | | SSE | dB | SSE | dB | SSE | dB | SSE | dB |
| tc1 (Fig. 3) | 128 radial | 3.35E3 | 16.10 | 3.71E3 | 15.26 | 3.57E3 | 15.55 | 3.02E3 | 16.69 |
| tc1 (Fig. 4) | 30 spiral | 1.12E4 | 6.40 | 1.61E4 | 3.76 | 1.48E4 | 4.57 | 9.62E3 | 8.17 |
| tl4 (Fig. 5) | 128 radial | 2.44E3 | 15.95 | 2.49E3 | 15.51 | 2.19E3 | 16.54 | 1.62E3 | 18.73 |
| tl4 (Fig. 6) | 30 spiral | 7.89E3 | 6.32 | 1.03E4 | 4.11 | 9.19E3 | 5.34 | 5.72E3 | 8.6 |
| dg1 (Fig. 7) | 128 radial | 2.35E3 | 12.10 | 3.38E3 | 10.04 | 2.99E3 | 10.99 | 2.24E3 | 12.94 |
| 038 (Fig. 8) | 128 radial | 2.55E3 | 15.02 | 2.47E3 | 14.32 | 2.1E3 | 15.65 | 1.49E3 | 17.95 |

The quantitative results obtained by the different interpolation methods involved are outlined in Table 1, except for the results of the two traditional interpolation techniques. These latter methods have always given worse results than the zero-filling reconstruction. For instance, for

the test image of Fig. 5 the cubic interpolation gives 2.7E3 for the SSE and 15.02 dB for the RMS, for the comparison with the original image, which are obviously worse than the ones obtained by zero-filling reconstruction. Concerning reconstruction performance qualitative results, they are all shown in Figs. 3–8. Both quantitative and qualitative results clearly demonstrate the superiority of the proposed supervised and unsupervised ANN interpolation approach in terms of MRI image reconstruction performance. Although, MLP based reconstruction is generally better than SOFM's reconstruction in terms of SSE and RMS errors, the pictures 3–8 show that SOFM produces only slightly worse reconstruction results. On the other hand, concerning Bayesian reconstruction, the initial results indicate that its performance is worse than that of MLP and slightly better than that obtained by unsupervised models, except in two cases.

## 6. Conclusions and future trends

A new methodology has been developed for reconstructing MRI images from sparsely sampled *k*-space data using MLP and SOFM interpolation techniques for estimating the missing samples. A detailed experimental study on a well organized MRI image database demonstrates that the proposed approach gives very promising results concerning reconstruction performance, compared to some traditional interpolation techniques in terms of both quantitative and qualitative evaluation. More specifically, the suggested approach leads to smaller MRI reconstruction error (SSE, RMS) than the zero-filling method as well as than the cubic or linear interpolation techniques. In addition, a preliminary comparison with the recently proposed Bayesian reconstruction indicates that the quantitative reconstruction results obtained by supervised neural models are favorably compared to the ones obtained by the Bayesian approach in terms of SSE and RMS. The unsupervised neural models, however, give slightly worse results than the Bayesian methodology in the majority of test images. Apart from the better reconstruction results, an advantage of neural estimation methodology is that, it is much faster than the Bayesian estimation approach (more than 20 times faster in terms of CPU time, for the test images of $256 \times 256$ dimensions). A disadvantage, however, of the proposed methodology is the hard work needed to select a representative training set of MRI images so that it could be universally applied for all MRI images. On the other hand, while Bayesian reconstruction seems to be able to be universally applied, it depends, however, on the prior knowledge function as well as on the Gaussian assumptions for the probability distributions involved, both of which might be not valid for all MRI images. Therefore, a much more extensive comparison is needed to reveal these advantages and disadvantages. What is more interesting, however, is to achieve a combination of these two approaches since ANN interpolation can supply Bayesian reconstruction with a better starting point for the optimization process.

## References

Barone, P., Sebastiani, G., 1992. A new method of magnetic resonance image reconstruction with short acquisition time and truncation artifact reduction. IEEE Trans. Med. Imaging 1, 250.

Basic Principles of MR Imaging, 1995. Philips Medical Systems, Best, The Netherlands.

Dologlou, I., Wajer, F.T.A.W., Fuderer, M., van Ormondt, D., 1996. Spiral MRI scan-time reduction through non-uniform angular distribution of interleaves and multichannel SVD interpolation. In: Proceedings of ISMRM Fourth Meeting, New York, p. 1489.

Fuderer, M., 1989. Ringing artefact reduction by an efficient likelihood improvement method. Proc. SPIE 1137, 84–90.

Herbert, T., Leahy, R., 1989. A generalized EM algorithm for 3-D Bayesian reconstruction from Poisson data using Gibbs priors. IEEE Trans. Med. Imaging 8, 194–202.

Lettington, A.H., Quong, Q.H., 1995. Image restoration using a lorentzian probability model. J. Modern Optics 42, 1367–1376.

Li, X., Hornak, J.P., 1994. $T_2$ calculations in MRI: linear versus nonlinear methods. J. Imag. Sci. & Technol. 38, 154–157.

Servoss, T.G., Hornak, J.P., 2000. Spatial–spatia–spectral imaging using a clinical MRI. Experimental NMR Conference, Asilomar, CA, April.

Smith, M.R., Nichols, S.T., Henkelman, R.M., Wood, M.L., 1986. Application of autoregressive modelling in magnetic resonance imaging to remove noise and truncation artifacts. Magn. Reson. Imaging 4, 257.

Stijnman, G.H.L.A., Graveron-Demilly, D., Wajer, F.T.A.W., van Ormondt, D., 1997. MR image estimation from sparsely sampled radial scans. Proc. ProRISC/IEEE Benelux workshop on circuits, systems and signal processing, Mierlo, The Netherlands, pp. 603–611.